




Effect of symmetry breaking of polarized light sea quarks on the nucleon and nuclear structure functions, and sum rules

Fatemeh Arbabifar¹ ,* Shahin Atashbar Tehrani² ,† and Hamzeh Khanpour^{3,4,2}  ‡

⁽¹⁾ *Department of Physics, Nasibeh campus, Farhangian University, P.O.Box 14665-889, Tehran, Iran*

⁽²⁾ *School of Particles and Accelerators, Institute for Research in Fundamental Sciences (IPM), P.O.Box 19395-5531, Tehran, Iran*

⁽³⁾ *AGH University of Science and Technology, Faculty of Physics and Applied Computer Science, Al. Mickiewicza 30, 30-055 Krakow, Poland*

⁽⁴⁾ *Department of Physics, University of Science and Technology of Mazandaran, P.O.Box 48518-78195, Behshahr, Iran*

(Dated: August 22, 2023)

In this study, we performed calculations and analyses of the structure functions of polarized nucleons and light nuclei, specifically ^3He and ^3H , using second-order Feynman diagrams. Our investigation focused on two main aspects: Firstly, we examined the symmetry properties of polarized light sea quarks. Secondly, we conducted a detailed investigation into the impacts of symmetry breaking on the structure functions of both nucleons and nuclei. To achieve this, we utilized the existing polarized Parton Distribution Functions (polarized PDFs) available in the literature. These PDFs were used to calculate and compare the polarized structure functions g_1 and g_2 of the nuclei. Additionally, we examined and analyzed the Bjorken and Efremov-Leader-Teryaev sum rules by utilizing the moments of the polarized structure functions. The Lorentz color force components, namely $F_E^{y,n}$ and $F_B^{y,n}$, are determined using the twist-2, twist-3, and twist-4 matrix elements. When symmetry breaking is applied, it is observed that they have similar magnitudes but opposite signs. Our theoretical predictions for the polarized structure functions of nucleons and light nuclei, taking into account the symmetry breaking of light sea quarks, exhibit better agreement with experimental data.

I. INTRODUCTION

Over the past years, the Deep Inelastic Scattering (DIS) of leptons from nucleons has been a widely used experimental method for investigating the internal structure of nucleons. Future lepton and hadron colliders, such as the Large Hadron-electron Collider (LHeC) [3], and the Future Circular Collider (FCC-he) [4] will also play an important role in investigating the internal structure of nucleons [1, 2]. Experimental groups such as E142, E143, COMPASS, HERMES, and JLAB have played a significant role in advancing our knowledge of nucleon structure by publishing a wealth of experimental results from collider experiments [5–10]. These experiments have focused on the DIS of polarized electrons by polarized nucleons and light nuclei, providing valuable insights into the nature of nucleon spin and its substructure.

The polarized structure functions of nucleons and nuclei provide useful information about the spin distribution of partons [11–15]. In the simple picture of the ^3He nuclei, all nucleons are in the S state wherein two protons with opposite spins exist, hence, their spins in the asymmetry are completely canceled and the nuclei polarization is determined solely by the neutron spin. Therefore, the use of ^3He targets in DIS experiments of leptons from polarized targets is common and is considered as an alternative target to the neutron. The same method applies

in the case of ^3H , where the neutrons are replaced with protons. However, in more precise calculations and by considering other components of the three-particle wave, such as S' and D states, the spins of the protons are no longer canceled in the ^3He structure function and must be taken into account.

In most published phenomenological models, the nucleon spin fractions carried by sea quarks are often assumed to be equal, and symmetry breaking is not taken into account, i.e. $\delta\bar{u} = \delta\bar{d} = \delta\bar{s}$ [19–38]. In some other phenomenological models, both flavor SU(2) and SU(3) symmetry breaking are taken into consideration, and hence, the nucleon spin fraction carried by the light sea quarks considered to be unequal as $\delta\bar{u} \neq \delta\bar{d} \neq \delta\bar{s}$ [14, 15, 39–45].

In the present work, both of the mentioned phenomenological methods are applied, and the polarized structure functions of nucleons and nuclei are calculated using some selected polarized PDF models available in the literature, namely NAAMY21 [25], AKS14 [44], DSSV09 [41], and BB10 [34].

In the most recent analysis, NAAMY21, the polarized Deep Inelastic Scattering (DIS) data is utilized, and the polarized PDFs of protons, neutrons, and deuterons are calculated at the next-to-leading order (NLO) approximation, without taking into account symmetry breaking. In other phenomenological model, AKS14, the asymmetry data from inclusive and semi-inclusive polarized Deep Inelastic Scattering (SIDIS) are utilized, and both flavor SU(2) and SU(3) symmetry breaking are taken into consideration. The QCD-PEGASUS software package [46] is employed in both analyses for the DGLAP (Dokshitzer-

* F.Arbabifar@cfu.ac.ir

† Atashbar@ipm.ir

‡ Hamzeh.Khanpour@cern.ch

Gribov-Lipatov-Altarelli-Parisi) evolution, and a QCD fit is conducted using the experimental polarized data. Both the NAAMY21 and AKS14 polarized PDFs are presented at the next-to-leading order (NLO) approximation in perturbative QCD.

In the present work, after calculating the moments of the polarized structure functions using the two mentioned polarized PDFs in the Mellin space, the DGLAP evolution equations [47] are solved. Then, using the Jacobi polynomials, the polarized structure functions of nucleons are calculated in the Bjorken x space. Finally, the polarized structure functions of the light nuclei Helium-3 (^3He) and Tritium (^3H) are extracted in the second approximation of the Feynman diagram. After applying the necessary corrections to the nuclei structure functions, we compare our results with the available experimental data for validation and comparison. Having the polarized structure functions of nucleons and nuclei, along with their moments, one can calculate various important quantities such as the Bjorken sum rule, Efremov-Leader-Teryaev sum rule, and the Lorentz color force components.

The organization of this paper is as follows: In Section II, we present the theoretical background of this study, including the polarized PDFs, the polarized structure functions, and a comparison with the available experimental data. In Section III, we discuss the polarized structure functions of nuclei, the associated corrections, and compare the results with experimental data. Sections IV and V present our results on the sum rules, specifically the Bjorken sum rule and the Efremov-Leader-Teryaev sum rule. In Section VI, we perform the calculation of the Lorentz color force components. Finally, Section VII provides a summary and conclusion of the work.

II. POLARIZED STRUCTURE FUNCTIONS OF NUCLEONS

In this section, we will present the theoretical framework for the calculation of the polarized structure functions of nucleons in the Mellin space. Following that, we will review the Jacobi polynomial method employed to transform the calculated structure functions from the Mellin space to the Bjorken x space. Additionally, we will provide a brief overview of previous studies on polarized PDFs, specifically the NAAMY21 and AKS14 models, which were utilized to compute the structure functions of nucleons and nuclei.

At the next-to-leading order (NLO) approximation, the polarized structure function of nucleons in Mellin space, denoted as $\mathcal{M}[xg_1, N](Q^2)$, can be expressed in terms of the polarized PDFs and the corresponding Wilson coefficient functions ΔC_i^N . Therefore, the polarized structure function is given by the following expression:

$$\begin{aligned} \mathcal{M}[xg_1^p, N](Q^2) &= \frac{1}{2} \sum_{q=u,d,s} e_q^2 \left\{ \left(1 + \frac{\alpha_s}{2\pi} \Delta C_q^N \right) \right. \\ &\quad \times [\delta q(N, Q^2) + \delta \bar{q}(N, Q^2)] \\ &\quad \left. + \frac{\alpha_s}{2\pi} 2\Delta C_g^N \delta g(N, Q^2) \right\}, \end{aligned} \quad (1)$$

$$\begin{aligned} \mathcal{M}[xg_1^n, N](Q^2) &= \mathcal{M}[xg_1^p, N](Q^2) - \frac{1}{6} \left(1 + \frac{\alpha_s}{2\pi} \Delta C_q^N \right) \\ &\quad \times (\delta u(N, Q^2) - \delta d(N, Q^2)), \end{aligned} \quad (2)$$

$$\begin{aligned} \mathcal{M}[xg_1^d, N](Q^2) &= \frac{1}{2} (\mathcal{M}[xg_1^p, N] + \mathcal{M}[xg_1^n, N]) \\ &\quad \times \left(1 - \frac{3}{2} \omega_D \right), \end{aligned} \quad (3)$$

for the proton (p), neutron (n) and deuteron (d), respectively.

In the equations above the $\omega_D = 0.058$ [48–50] and the Wilson coefficient ΔC_q^N and ΔC_g^N can be found in [47], and written as follows,

$$\begin{aligned} \Delta C_q^N &= \frac{4}{3} \left\{ -S_2(N) + (S_1(N))^2 + \left(\frac{3}{2} - \frac{1}{N(N+1)} \right) \right. \\ &\quad \times \left. S_1(N) + \frac{1}{N^2} + \frac{1}{2N} + \frac{1}{N+1} - \frac{9}{2} \right\}, \end{aligned} \quad (4)$$

$$\Delta C_g^N = \frac{1}{2} \left[-\frac{N-1}{N(N+1)} (S_1(N) + 1) - \frac{1}{N^2} + \frac{2}{N(N+1)} \right], \quad (5)$$

with $S_1(n) = \sum_{j=1}^n \frac{1}{j} = \psi(n+1) + \gamma_E$, $S_2(n) = \sum_{j=1}^n \frac{1}{j^2} = \left(\frac{\pi^2}{6} \right) - \psi'(n+1)$, $\psi(n) = \Gamma'(n)/\Gamma(n)$, $\gamma_E = 0.577216$ and $\psi'(n) = d^2 \ln \Gamma(n)/dn^2$.

It is important to note that the structure function of neutrons, defined through Eq. 2, takes into account symmetry breaking, meaning that the contribution of sea quarks is considered. However, if the symmetry of light sea quarks is neglected, the second term subtracted from the proton structure function can be replaced by $\delta u_v(N, Q^2) - \delta d_v(N, Q^2)$.

After determining the moments of the structure functions, they can be transformed to the Bjorken x space using the Jacobi polynomials [20]. The transformation is given by the following expression:

$$x g_1(x, Q^2) = x^\beta (1-x)^\alpha \sum_{n=0}^{N_{\max}} a_n(Q^2) \Theta_n^{\alpha, \beta}(x), \quad (6)$$

where the maximum order of expansion is denoted by N_{\max} , and the index n refers to the order of expansion.

Two free parameters α and β are chosen to make the fastest convergence for the series in Eq. 6. The $a_n(Q^2)$ as Jacobi moment discloses the dependence of polarized structure functions on Q^2 . By using the Jacobi polynomials, one can factor out from the structure function a weight function $w^{\alpha,\beta}(x) \equiv x^\beta(1-x)^\alpha$. Hence, the Jacobi polynomials $\Theta_n^{\alpha,\beta}(x)$ can be written as the following expansion:

$$\Theta_n^{\alpha,\beta}(x) = \sum_{j=0}^n c_j^{(n)}(\alpha, \beta) x^j. \quad (7)$$

It can be shown that the expansion coefficient $c_j^{(n)}(\alpha, \beta)$ is given by a combination of Gamma Γ function in terms of n , α and β parameters [51].

The following orthogonality relation is satisfied by the Jacobi polynomials with the weight function $w^{\alpha,\beta}(x)$,

$$\int_0^1 dx x^\beta (1-x)^\alpha \Theta_n^{\alpha,\beta}(x) \Theta_l^{\alpha,\beta}(x) = \delta_{n,l}. \quad (8)$$

Based on the orthogonality condition, the Jacobi moments $a_n(Q^2)$ can be obtained as [20, 53, 54]:

$$\begin{aligned} a_n(Q^2) &= \int_0^1 dx x g_1(x, Q^2) \Theta_n^{\alpha,\beta}(x) \\ &= \sum_{j=0}^n c_j^{(n)}(\alpha, \beta) \mathcal{M}[xg_1, j+2](Q^2), \end{aligned} \quad (9)$$

where the $\mathcal{M}[xg_1, j+2](Q^2)$ is the Mellin transform of the $xg_1(x, Q^2)$ from Eqs. 1, 2 and 3, which is given by,

$$\mathcal{M}[xg_1, N](Q^2) = \int_0^1 dx x^{N-2} xg_1(x, Q^2), \quad (10)$$

Now by substituting Eq. 9 into Eq. 6 the polarized structure function $xg_1(x, Q^2)$, based on Jacobi polynomial expansion method, can be constructed. Therefore the following expression for $xg_1(x, Q^2)$ could be obtained,

$$\begin{aligned} xg_1(x, Q^2) &= x^\beta(1-x)^\alpha \sum_{n=0}^{N_{\max}} \Theta_n^{\alpha,\beta}(x) \\ &\times \sum_{j=0}^n c_j^{(n)}(\alpha, \beta) \mathcal{M}[xg_1, j+2](Q^2). \end{aligned} \quad (11)$$

where N_{\max} is considered to be 9, and α and β are fixed to 3 and 0.5, respectively [20, 23, 24, 39].

The polarized PDFs of the NAAMY21 and AKS14 are depicted in Figures 1 and 2, respectively.

It is worth highlighting once again that the AKS14 model also conducted an additional analysis that included a positive polarized gluon to explore the impact of SU(2) and SU(3) symmetry breaking, as well as the

effect of SIDIS data on the polarized gluon distribution. In Figs. 3 and 4 we show the polarized PDFs obtained from AKS14 and NAAMY21 in comparison with experimental data from COMPASS [55] and HERMES [8] experiments. The results of two other available models, DSSV09 [41] and BB10 [34], are also shown for comparison. To calculate the $\delta q/q$ in Fig 4, the most recent unpolarized PDFs from CT18 [52] is used.

Considering the results presented in Figures 3 and 4, several remarks can be made. As shown in these plots, in general, the compatibility of the AKS14 model with the experimental data and their error is better than those of NAAMY21, more especially for the case of δs . However, it is important to note that the compatibility of the data with the NAAMY21 model is also good.

As can be seen, the DSSV09 results which come from the analysis with symmetry breaking consideration are mostly close to the AKS14 curves and both are in agreement with the experimental data. However, due to the wide dispersion of the related data, the plots might not be able to support them as one may expect. Also it is obvious that the results of BB10, with no symmetry breaking, is closer to the NAAMY21. For the case of $x\delta\bar{u} - x\delta\bar{d}$, both the AKS14 and DSSV09 models show the same level of compatibility and are in agreement with the COMPASS data. For the specific parton species, it is observed that both the AKS14 and DSSV09 models demonstrate a better agreement with the COMPASS data in terms of $x\delta\bar{u}$ and $x\delta\bar{d}$ compared to other groups. Significant deviations from the COMPASS data are observed for the NAAMY21 and BB10 for the case of $x\delta\bar{u}$ and $x\delta s$.

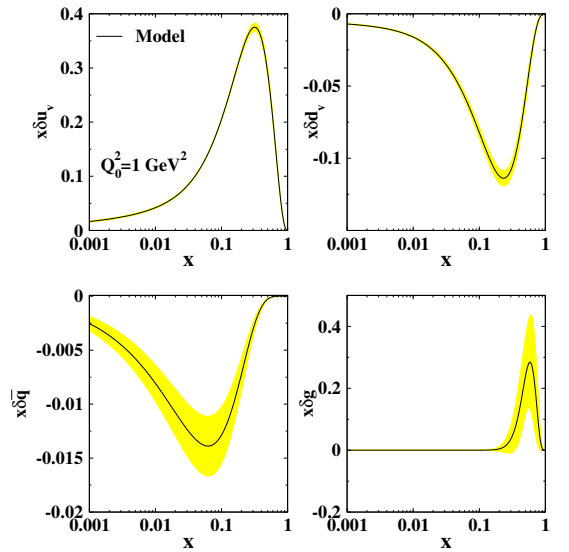


Figure 1: The polarized PDFs from NAAMY21 [25] model at $Q_0^2 = 1 \text{ GeV}^2$ in NLO approximation, considering $\delta\bar{q} = \delta\bar{u} = \delta\bar{d} = \delta\bar{s}$.

With the moment expressions for the polarized structure functions of the proton, neutron, and deuteron pre-

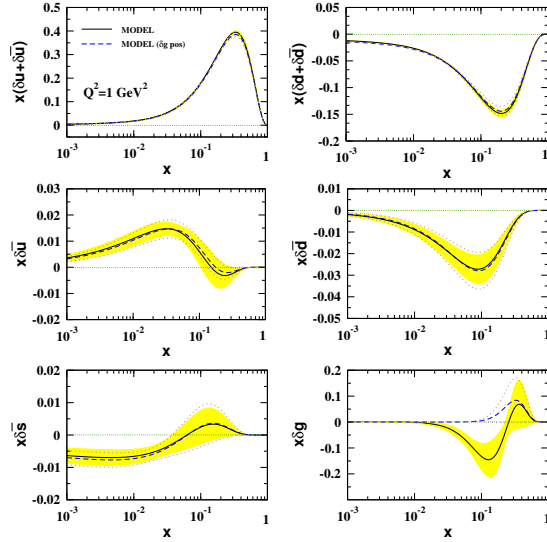


Figure 2: The polarized PDFs from AKS14 [44] model at $Q_0^2 = 1 \text{ GeV}^2$ at NLO approximation, considering $\delta\bar{u} \neq \delta\bar{d} \neq \delta\bar{s}$. Solid line indicates the AKS14 model in sign changing gluon scenario, dashed line denotes the AKS14 model in positive gluon scenario.

sented in Eqs.1, 2, and 3, respectively, and utilizing the Jacobi polynomials, the structure functions can be calculated in the Bjorken x space. Figs. 5, 6, and 7 show the comparison of the structure functions of proton, neutron, and deuteron with E143 experimental data [6]. We show both the absolute distributions (upper panel) and the data/theory ratios (down panel) for detailed comparison. In order to correctly assess whether or not the different theoretical results are statistically different one from the other, and to examine the compatibility with the data, the theory predictions for different polarized PDFs sets are also displayed with error bands. The results from DSSV09 and BB10 are also shown and compared.

In general, as observed from these plots, the nucleon polarized structure functions generated by the AKS14 model, which takes into account symmetry breaking, are quite close to the DSSV09 polarized structure functions, where SU(2) and SU(3) symmetry breaking is also considered.

Focusing on the comparison with the proton polarized structure function shown in Figure 5, one can observe a larger error band for the AKS14 model. The theoretical prediction of the AKS14 model and the data are compatible over the range of medium to small values of x . Although, differences are also seen at large x , they are always compatible within uncertainties. As one can see from the data/theory ratios (down panel), the compatibility of AKS14 theory prediction and the E143 experimental data are better than those of NAAMY21 at large x . The compatibility of the AKS14 and NAAMY21 theory predictions with the data is similar for small values of x .

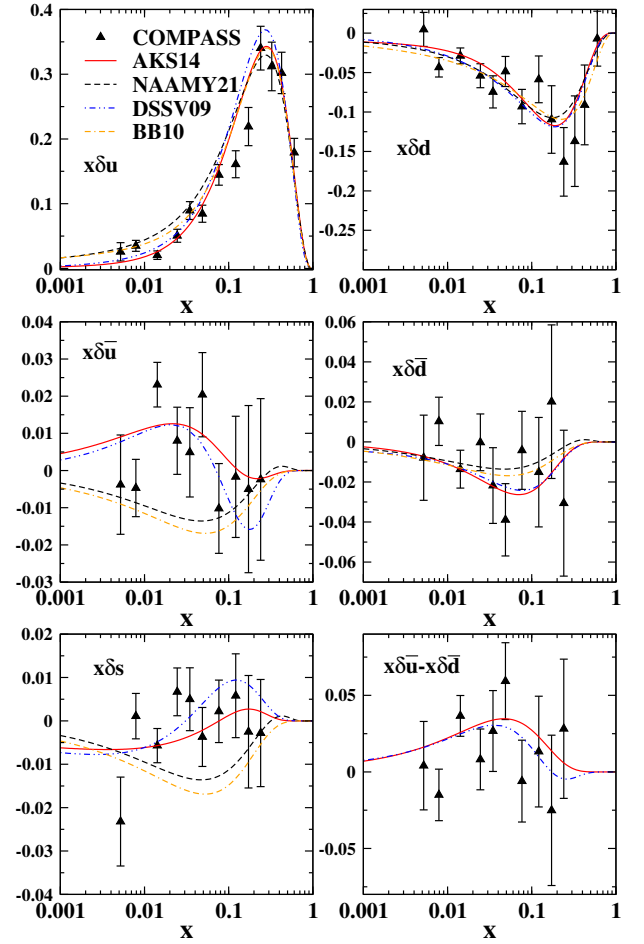


Figure 3: The NLO polarized PDFs from AKS14, NAAMY21, DSSV09 [41] and BB10 [34] in comparison with COMPASS [55] experimental data at $Q^2 = 3 \text{ GeV}^2$.

In Fig. 6, we present a comparison of the neutron polarized structure function with data from the E143 Collaboration. Our analysis indicates that both the AKS14 and NAAMY21 curves demonstrate a good level of agreement with the central points of the experimental data. Specifically, for small to medium values of x , the theoretical predictions of both the AKS14 and NAAMY21 models exhibit better accordance with the data, considering the uncertainties, when compared to other models. However, it is important to note that deviations from the experimental data can be observed for both models, particularly at large values of x .

Finally, focusing on the deuteron polarized structure function in Fig. 7, it can be observed that the NLO prediction of the structure function calculated from the AKS14 model is in good agreement with the E143 experimental data across the entire range of x . The DSSV09 polarized structure functions are also seen to be close to the AKS14 curves, as both models account for SU(2) and SU(3) symmetry breaking. Comparing with the NAAMY21

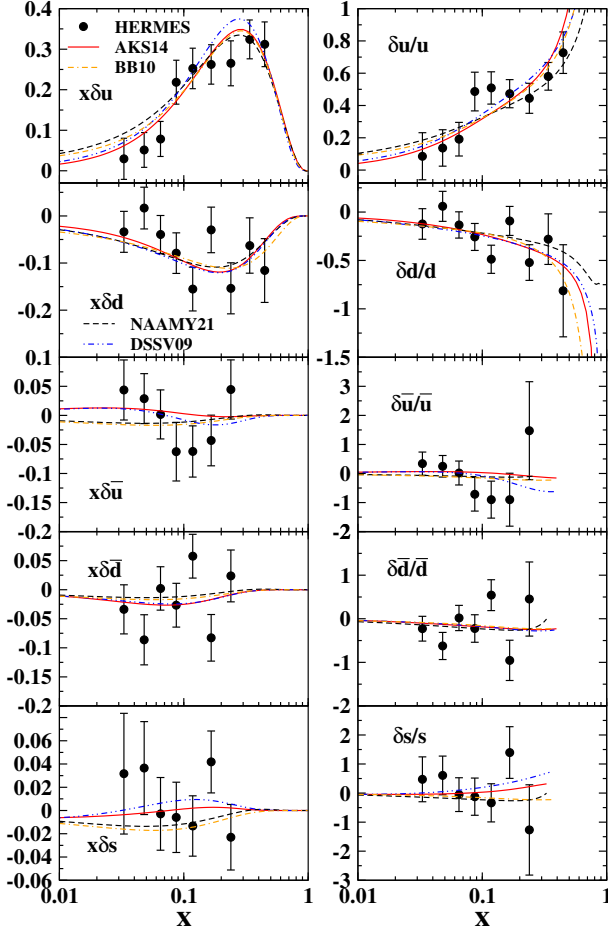


Figure 4: Same as Fig. 3 but this time in comparison with HERMES experimental data [8] at $Q^2 = 2.5 \text{ GeV}^2$.

model, the data/theory ratios (bottom panel) indicate that the compatibility of the AKS14 theory prediction is better. This difference is particularly evident at very large and small values of x , taking into account the uncertainties.

In Table. I, we present the value of the moments of nucleon polarized structure functions at 3 GeV^2 for AKS14, NAAMY21 polarized PDFs. Comparing the values of $\Gamma_1^p = 0.139 \pm 0.003 \pm 0.009 \pm 0.005$, $\Gamma_1^n = -0.041 \pm 0.006 \pm 0.011 \pm 0.005$, and $\Gamma_1^d = 0.049 \pm 0.003 \pm 0.004 \pm 0.004$, reported by COMPASS experimental group [7] with the values reported in Table. I, it is observed that the values of moments of neutron and deuteron polarized structure functions, when symmetry breaking is taken into account in the AKS14, are more compatible with COMPASS results. For the case of proton, the value extracted from NAAMY21 is in better agreement with the COMPASS results.

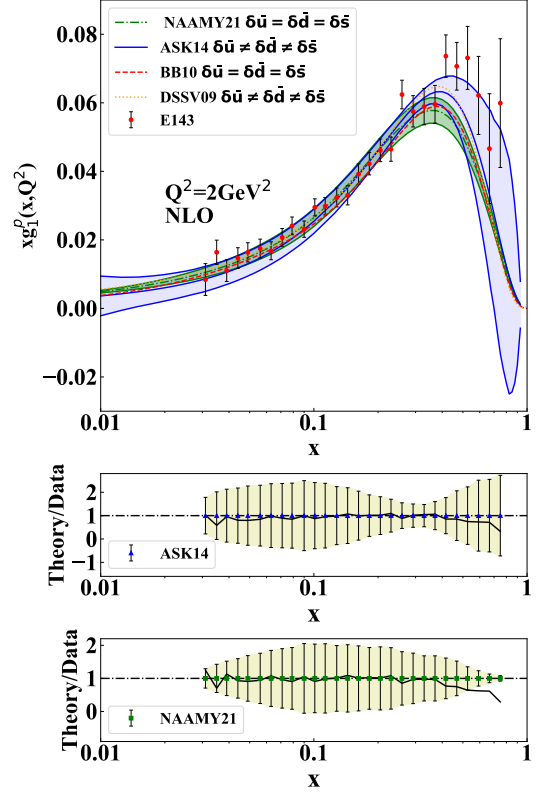


Figure 5: The NLO prediction for the proton polarized structure function calculated using the AKS14, NAAMY21, DSSV09, BB10 in comparison with E143 experimental data [6] at $Q^2 = 2 \text{ GeV}^2$.

	Γ_1^p	Γ_1^n	Γ_1^d
AKS14	0.1273 ± 0.0003	-0.0374 ± 0.00035	0.0406 ± 0.00032
NAAMY21	0.1322 ± 0.0053	-0.0554 ± 0.0056	0.0350 ± 0.0050

Table I: The first momentum of the nucleon polarized structure functions calculated using AKS14 and NAAMY21 polarized PDFs.

III. POLARIZED STRUCTURE FUNCTIONS OF NUCLEI

This section emphasizes the calculation of the polarized structure functions of light nuclei, as well as the impact of the symmetry breaking of polarized light sea quarks on the agreement between theory and experimental data. The calculations in the previous section showed that the polarized PDFs, polarized structure functions of proton, neutron, deuteron, and their first moments obtained from the AKS14 polarized PDFs, in general, have better compatibility with the experimental data from COMPASS [7, 55], and E143 [6].

In the following section, we analyze the polarized structure functions of light nuclei Helium-3 ^3He and Tritium

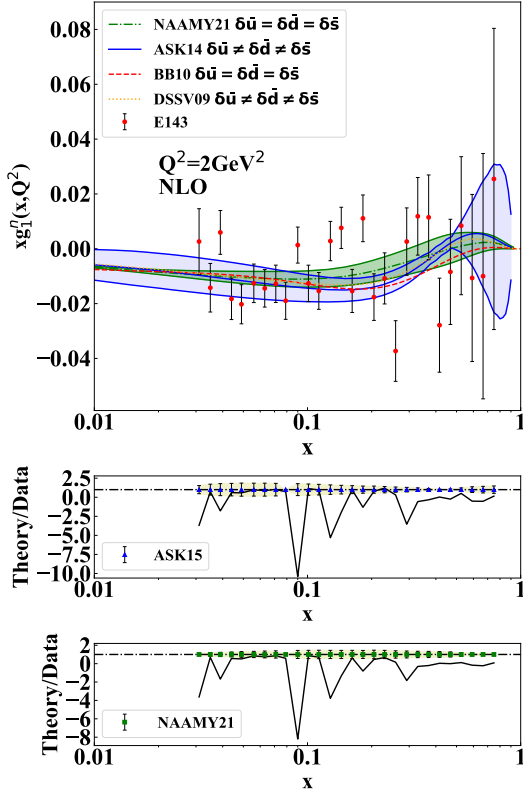


Figure 6: The neutron polarized structure function at $Q^2 = 2 \text{ GeV}^2$, compared with AKS14, NAA MY21, DSSV09, BB10 and E143 experimental data [6].

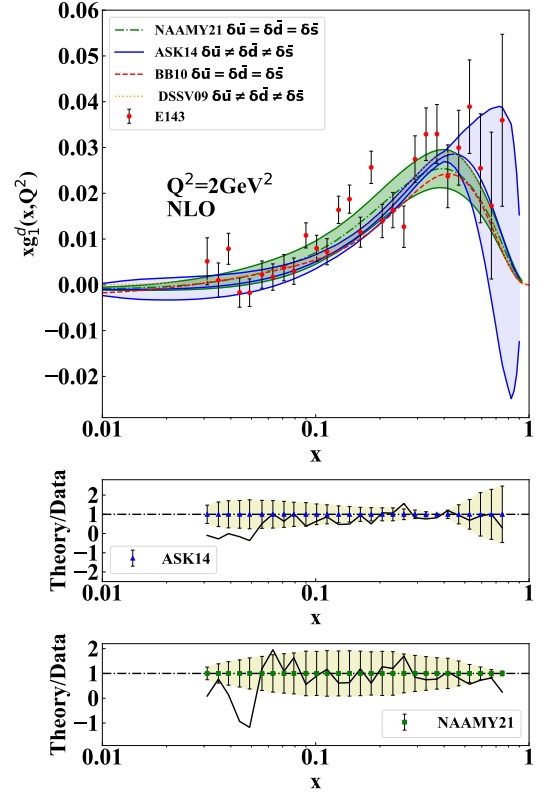


Figure 7: The deuteron polarized structure function at $Q^2 = 2 \text{ GeV}^2$, compared with AKS14, NAA MY21, DSSV09, BB10 and E143 experimental data [6].

^3H . These two are trivalent light nuclei that, respectively, consist of two protons plus one neutron and two neutrons plus one proton. Despite their wave function at ground state level is in the S state, the higher states S' and D can be also found in a more realistic definition. At S' and D states, the spin contributions of two protons in Helium-3 or the two neutrons in Tritium are not canceled and must be considered in the calculations. The calculation of the polarized structure function can be performed using the contribution of proton and neutron polarized structure function in addition to the spin-dependent nucleon light-cone momentum distributions $\Delta f_{^3\text{He}}^p$ and $\Delta f_{^3\text{He}}^n$ [16–18, 56, 62]. They are given by,

$$g_1^{^3\text{He}} = \int_x^3 \frac{dy}{y} \Delta f_{^3\text{He}}^n(y) g_1^n(x/y) + 2 \int_x^3 \frac{dy}{y} \Delta f_{^3\text{He}}^p(y) g_1^p(x/y), \quad (12)$$

$$g_1^{^3\text{H}} = \int_x^3 \frac{dy}{y} \Delta f_{^3\text{He}}^n(y) g_1^n(x/y) + 2 \int_x^3 \frac{dy}{y} \Delta f_{^3\text{He}}^p(y) g_1^p(x/y). \quad (13)$$

It is noticeable that because of isospin symmetry, the light cone momentum distribution $\Delta f_{^3\text{He}}^p$ and $\Delta f_{^3\text{H}}^n$ are equal in size. In Fig. 8 we show the spin-dependent nucleon light-cone momentum distributions $\Delta f_{^3\text{He}}^n$ and $\Delta f_{^3\text{He}}^p$ [56] as a function of y . For the calculation of $\Delta f_{^3\text{He}}^n$ and $\Delta f_{^3\text{He}}^p$, we utilized the PEST nucleon-nucleon (N-N) interaction which is derived from the Paris N-N potential [57].

In addition to the correction discussed above, various calculations show that the main contribution to the g_1 should originate from the $n \rightarrow \Delta^0$ non-diagonal transition in ^3He and from the $p \rightarrow \Delta^+$ non-diagonal transition in ^3H case [58–61].

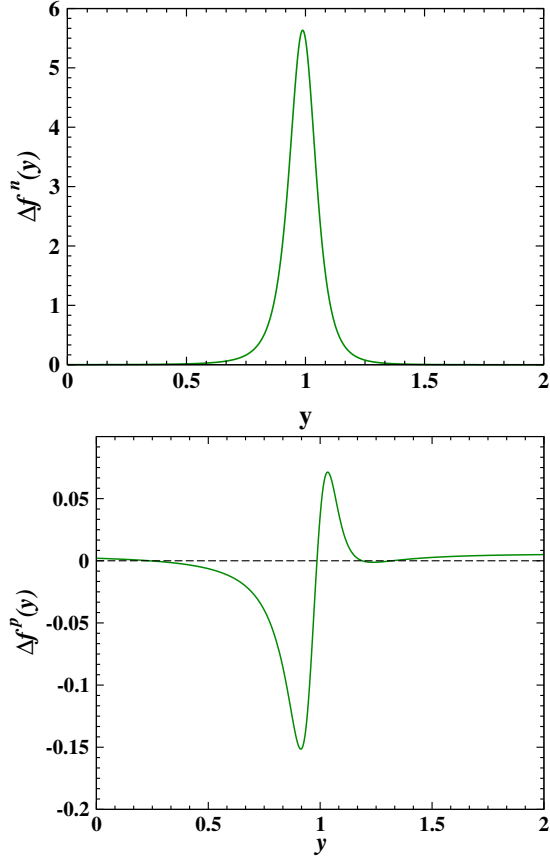


Figure 8: The Spin-dependent nucleon light-cone momentum distributions $\Delta f_{3\text{He}}^p$ and $\Delta f_{3\text{He}}^n$ [56] as a function of y .

$$\begin{aligned}
g_1^{3\text{He}}(x, Q^2) = & \int_x^3 \frac{dy}{y} \Delta f_{3\text{He}}^n(y) g_1^n(x/y, Q^2) + \\
& 2 \int_x^3 \frac{dy}{y} \Delta f_{3\text{He}}^p(y) g_1^p(x/y, Q^2) \\
& + 4P_{p \rightarrow \Delta^+} g_1^{p \rightarrow \Delta^+}(x, Q^2) + 2P_{n \rightarrow \Delta^0} g_1^{n \rightarrow \Delta^0}(x, Q^2), \quad (14)
\end{aligned}$$

$$\begin{aligned}
g_1^{3\text{H}}(x, Q^2) = & \int_x^3 \frac{dy}{y} \Delta f_{3\text{He}}^n(y) g_1^p(x/y, Q^2) + \\
& 2 \int_x^3 \frac{dy}{y} \Delta f_{3\text{He}}^p(y) g_1^n(x/y, Q^2) \\
& - 2P_{n \rightarrow \Delta^0} g_1^{p \rightarrow \Delta^+}(x, Q^2) - 4P_{p \rightarrow \Delta^+} g_1^{n \rightarrow \Delta^0}(x, Q^2), \quad (15)
\end{aligned}$$

As a result, the structure functions $g_1^{n \rightarrow \Delta^0}$ and $g_1^{p \rightarrow \Delta^+}$ should be considered in the calculations, which will lead

to a correction for the three particle nuclei structure function. Regarding to the model-independent equation [62], we have

$$g_1^{p \rightarrow \Delta^+}(x, Q^2) = g_1^{n \rightarrow \Delta^0}(x, Q^2) = \frac{2\sqrt{2}}{5}(g_1^p - 4g_1^n), \quad (16)$$

and the polarized structure function equation will be written as,

$$\begin{aligned}
g_1^{3\text{He}} = & \int_x^3 \frac{dy}{y} \Delta f_{3\text{He}}^n(y) g_1^n(x/y) + 2 \int_x^3 \frac{dy}{y} \Delta f_{3\text{He}}^p(y) g_1^p(x/y) \\
& - 0.014(g_1^p(x) - 4g_1^n(x)), \quad (17)
\end{aligned}$$

and

$$\begin{aligned}
g_1^{3\text{H}} = & \int_x^3 \frac{dy}{y} \Delta f_{3\text{He}}^n(y) g_1^p(x/y) + 2 \int_x^3 \frac{dy}{y} \Delta f_{3\text{He}}^p(y) g_1^n(x/y) \\
& + 0.014(g_1^p(x) - 4g_1^n(x)). \quad (18)
\end{aligned}$$

At high energy levels or at low values of Bjorken x , the virtual photon can interact with multiple nucleons coherently. This behavior is apparent in nuclear targets. Nuclear shadowing and antishadowing are examples of these coherent effects [62, 63]. According to the shadowing and antishadowing correction, the Helium-3 and Tritium nuclei polarized structure functions can be rewritten as,

$$\begin{aligned}
g_1^{3\text{He}} = & \int_x^3 \frac{dy}{y} \Delta f_{3\text{He}}^n(y) g_1^n(x/y) + 2 \int_x^3 \frac{dy}{y} \Delta f_{3\text{He}}^p(y) g_1^p(x/y) \\
& - 0.014(g_1^p(x) - 4g_1^n(x)) + a(x)g_1^n(x) + b(x)g_1^p(x), \quad (19)
\end{aligned}$$

and

$$\begin{aligned}
g_1^{3\text{H}} = & \int_x^3 \frac{dy}{y} \Delta f_{3\text{He}}^n(y) g_1^p(x/y) + 2 \int_x^3 \frac{dy}{y} \Delta f_{3\text{He}}^p(y) g_1^n(x/y) \\
& + 0.014(g_1^p(x) - 4g_1^n(x)) + a(x)g_1^n(x) + b(x)g_1^p(x), \quad (20)
\end{aligned}$$

where $a(x)$ and $b(x)$ functions describe the shadowing and anti-shadowing effect as a function of x and Q^2 [62]. Since the current experimental data do not cover very small values of x considerably, the corrections from shadowing ($10^{-4} \leq x \leq 0.03 - 0.07$) and ($0.03 - 0.07 \leq x \leq 0.2$) anti-shadowing can be completely ignored in the calculations of polarized nuclei [10]. However, the calculations of Refs. [62, 63] have shown that these effects are quite significant and impact the extraction of the nucleon polarized structure functions at small values of Bjorken x .

According to Eqs. 17 and 18, the Helium-3 and Tritium polarized structure functions are extracted at 5 GeV^2 and 2.5 GeV^2 respectively and they are shown in Figs. 9 and 10.

Polarized structure functions of ^3He and ^3H at NLO and NNLO from NAAMY21 and KTA17 [39] polarized PDFs, both concerning symmetry of light sea quarks, are compared with AKS14 [44] model at NLO concerning symmetry breaking of light sea quarks.

In Fig.9, we also include the E142[5] and JLAB [64] experimental data for comparison. As shown in this figure, the theory prediction from the AKS14 model, even though it is similar to that of NAAMY21, exhibits slightly better compatibility with the experimental results across most of the Bjorken x region covered by the data. This compatibility is particularly emphasized for larger values of x ($x > 0.1$) within the uncertainty bands.

In Fig. 10 and for the case of g_1^H polarized structure functions, one can see that the difference between the curves with and without considering symmetry breaking is noticeable, especially at low value of x .

Fig. 11 shows the comparison of $x^2 g_1^{^3\text{He}}$ polarized structure function in comparison with E142 [5], JLAB04 [64], JLAB03 [65], and JLAB16 [10] experimental data at different energies in the range of $1.1 < Q^2 < 5.89 \text{ GeV}^2$. Based on this plot, it can be concluded that the AKS14 model exhibits comparable agreement to the other models within the region of $0.1 \leq x \leq 0.4$. For higher values of x , the NAAMY21 and KTA17 models show better compatibility with the experimental data points. However, it should be noted that both the AKS14 and NAAMY21 models remain compatible within the given uncertainties throughout the entire range.

The Wandzura-Wilczek g_2 structure function [66] can be calculated as $g_2^{WW}(x) = -g_1(x) - \int_x^1 \frac{dy}{y} g_1(y)$, and for the case of Helium-3 and Tritium structure functions, they are given by:

$$\begin{aligned} g_2^{^3\text{He}} = & \int_x^3 \frac{dy}{y} \Delta f_{^3\text{He}}^n(y) g_2^n(x/y) \\ & + 2 \int_x^3 \frac{dy}{y} \Delta f_{^3\text{He}}^p(y) g_2^p(x/y) \\ & - 0.014 \left(g_2^p(x) - 4g_2^n(x) \right), \end{aligned} \quad (21)$$

and

$$\begin{aligned} g_2^{^3\text{H}} = & \int_x^3 \frac{dy}{y} \Delta f_{^3\text{He}}^n(y) g_2^n(x/y) \\ & + 2 \int_x^3 \frac{dy}{y} \Delta f_{^3\text{He}}^p(y) g_2^p(x/y) \\ & + 0.014 \left(g_2^p(x) - 4g_2^n(x) \right). \end{aligned} \quad (22)$$

Figs. 12 and 13 display the polarized structure of $g_2^{^3\text{He}}$ extracted from AKS14 and NAAMY21 at NLO, and

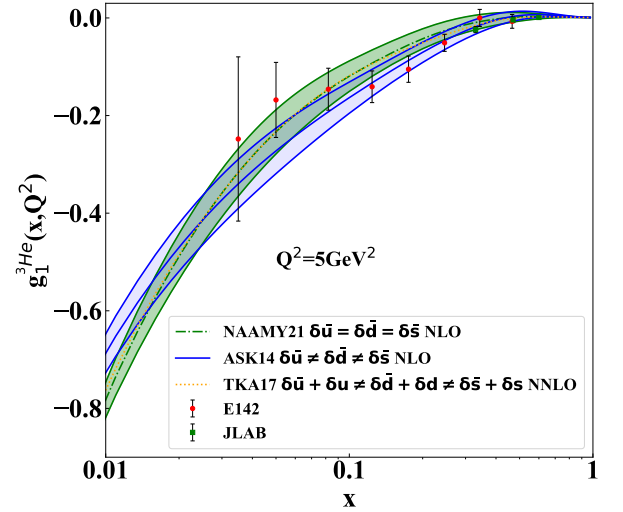


Figure 9: The theory prediction for $g_1^{^3\text{He}}$ polarized structure functions at NLO and NNLO approximation from NAAMY21, AKS14 and KTA17 in comparison with experimental data from E142 [5] and JLAB [64].

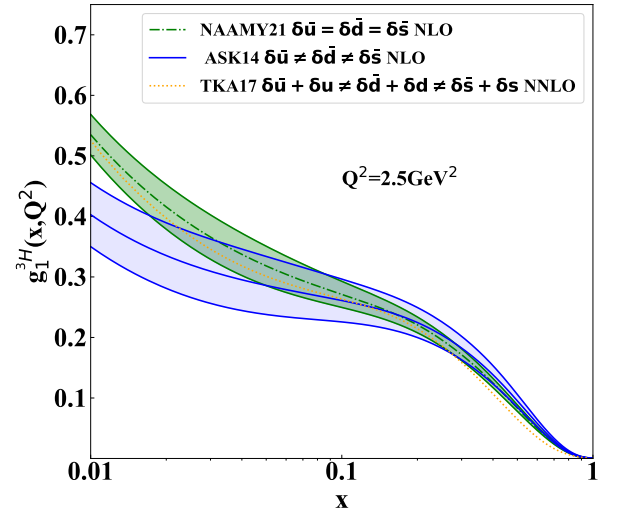


Figure 10: Same as Fig. 9 but this time for the $g_1^{^3\text{H}}$ polarized structure functions.

KTA17 [39] at the NNLO approximation compared to the JLAB04 [9] and JLAB16 [10] experimental data. Although the curves are not exactly the same, a similar agreement in the behavior of three models in comparison with the experimental data of JLAB04 and JLAB16 and their error bar is observed.

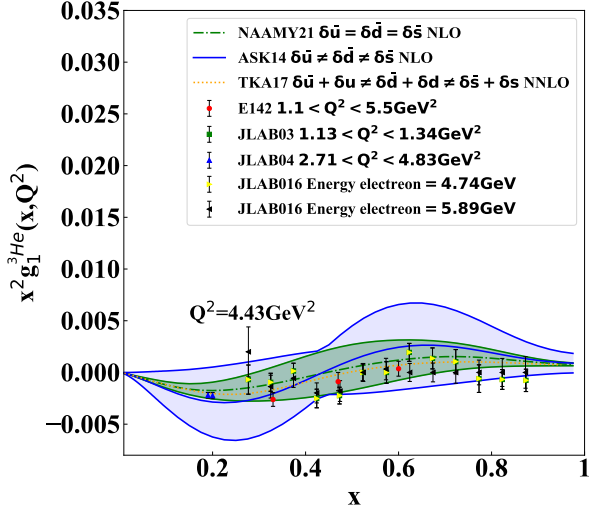


Figure 11: Same as Fig. 9 but this time for the $x^2 g_1^{3\text{He}}$ polarized structure functions in comparison with experimental data from E142 [5], JLAB04 [64], JLAB03 [65] and JLAB16 [10].

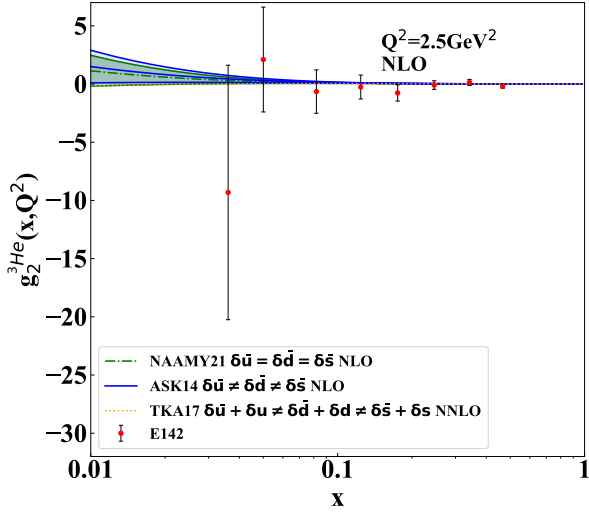


Figure 12: Same as Fig. 9 but this time for the $g_2^{3\text{He}}$ polarized structure functions in comparison with E142 experimental data [5].

IV. BJORKEN SUM RULE

To quantify the nuclear corrections as expressed in Eqs. 17 and 18 we use the ratio known as η . Bjorken sum rule evaluates the difference between the first moment between Helium and Tritium polarized structure functions. It is given by,

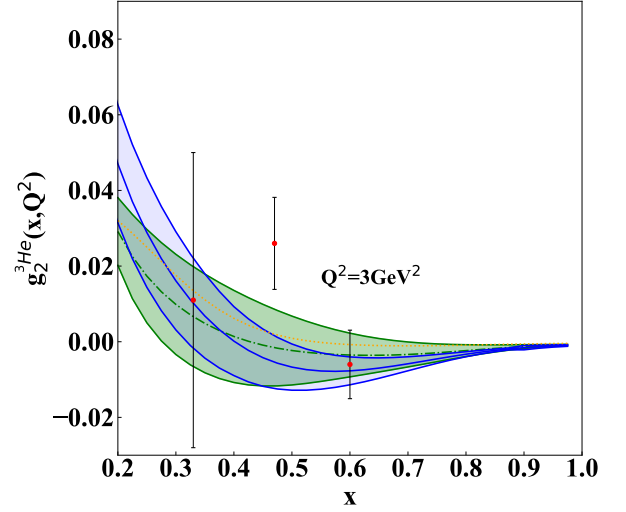


Figure 13: Same as Fig. 9 but this time for the $g_2^{3\text{He}}$ polarized structure functions in comparison with the JLAB experimental data [64].

$$\int_0^3 [g_1^{3\text{H}}(x, Q^2) - g_1^{3\text{He}}(x, Q^2)] dx = \frac{1}{6} g_A|_{\text{triton}} [1 + \mathcal{O}(\frac{\alpha_s}{\pi})], \quad (23)$$

where $g_A|_{\text{triton}} = 1.211 \pm 0.002$ [67]. According to the Bjorken sum rule [68] for proton and neutron without nuclei constraint we have

$$\int_0^1 [g_1^p(x, Q^2) - g_1^n(x, Q^2)] dx = \frac{1}{6} g_A [1 + \mathcal{O}(\frac{\alpha_s}{\pi})], \quad (24)$$

where $g_A = 1.2670 \pm 0.0035$ [69]. Finally the ratio η can be written as,

$$\eta \equiv \frac{g_A|_{\text{triton}}}{g_A} = \frac{\int_0^3 [g_1^{3\text{H}}(x, Q^2) - g_1^{3\text{He}}(x, Q^2)] dx}{\int_0^1 [g_1^p(x, Q^2) - g_1^n(x, Q^2)] dx} = 0.956 \pm 0.004. \quad (25)$$

In the calculations, we obtained a value of 0.936 ± 0.002 for NAAMY21 model and 0.954 ± 0.003 for AKS14. This result indicates that the analysis taking into account symmetry breaking produces a value of the ratio η that is closer to the Bjorken sum rule compared to the analysis that neglects symmetry breaking.

V. EFREMOV-LEADER-TERYAEV (ELT) SUM RULE

The Efremov-Leader-Teryaev (ELT) sum rule can be derived by integrating the valence part of the g_1 and g_2 structure functions over the Bjorken x variable in the limit $m_q \rightarrow 0$ [70]. The ELT sum rule is expressed as follows:

$$\int_0^1 x[g_1^V(x) + 2g_2^V(x)]dx = 0. \quad (26)$$

where $g_{1(2)}^V$ denotes the valence quark contributions to the $g_{1(2)}$. When considering the symmetry of light sea quarks and assuming they carry an equal fraction of the spin in protons and neutrons, the Efremov-Leader-Teryaev (ELT) sum rule can be written as follows:

$$\int_0^1 x[g_1^p(x) - g_1^n + 2(g_2^p(x) - g_2^n(x))]dx = 0. \quad (27)$$

The values obtained 0.01017 ± 0.00004 and -0.030763 ± 0.0004071 from NAAMY21 and AKS14 respectively. It seems the consideration of the light sea quarks symmetry breaking, the ELT sum rule is derived directly from Eq. 26. The value of the left hand side of above equation is obtained -0.011 ± 0.008 from E155 [71] analysis at $Q^2 = 5 \text{ GeV}^2$. The symmetry breaking makes the results negative, however are of a similar magnitude. Also it is concluded that disregarding the symmetry of $\delta\bar{u}$, $\delta\bar{d}$ and $\delta\bar{s}$ can be effective on the magnitude of ELT sum rule to be far from zero.

VI. LORENTZ COLOR FORCE COMPONENTS

The force exerted by the probing quark on the struck quark in the DIS process, perpendicular to the direction of motion, is referred to as the Lorentz color force. It is divided into electric and magnetic components [72]

$$F_E^{y,n} = -\frac{M_n^2}{6}(2d_2^n + f_2^n), \quad (28)$$

$$F_B^{y,n} = -\frac{M_n^2}{6}(4d_2^n - f_2^n). \quad (29)$$

Here d_2^n is twist-3 matrix element and can be evaluated via

$$d_2(Q^2) = \int_0^1 x^2[2g_1(x, Q^2) + 3g_2(x, Q^2)]dx, \quad (30)$$

and f_2^n is twist-4 matrix element and can be extracted from the first moment equation of $g_1(x, Q^2)$ [73]

$$\eta_1 \equiv \int_0^1 g_1(x, Q^2)dx \quad (31)$$

$$= \mu_2 + \frac{M^2}{9Q^2}(a_2 + 4d_2 + 4f_2) + \mathcal{O}\left(\frac{1}{Q^4}\right). \quad (32)$$

The quantity μ_2 is known as twist-2 contribution

$$\mu_2(Q^2) = C_{ns}(Q^2) \left(-\frac{1}{12}g_A + \frac{1}{36}a_8 \right) + C_s(Q^2)\Delta\Sigma, \quad (33)$$

in which C_{ns} and C_s are the nonsinglet and singlet Wilson coefficients [74]. g_A and a_8 are respectively the flavor-triplet and the octet axial charge and $\Delta\Sigma$ denotes the singlet axial current [75, 76]. The quantity a_2 is the third moment of g_1 known as $a_2 = \int x^2 g_1 dx$.

In Table. II, we present the calculated values for the d_2^n , f_2^n and a_2^n using two models of AKS14 and NAAMY21. The corresponding value from JLAB experiment [10] also has been shown as well.

Table. III presents the calculated magnetic and electric Lorentz color force components calculated from AKS14 and NAAMY21 models. The measured values from JLAB for Lorentz color force components [10] also presented in Table. III for comparison.

As one can see, the magnitudes of $F_B^{y,n}$ and $F_E^{y,n}$ extracted from the AKS14 QCD analysis, which takes into account the symmetry breaking of light sea quarks, exhibit good agreement with the measured values from the JLAB experiment. In addition, the calculated Lorentz color forces denoted by $F_B^{y,n}$ and $F_E^{y,n}$ are in same size with a different signs as expected from QCD prediction [72]. The magnitudes of these two forces, extracted from NAAMY21 QCD analysis with no symmetry breaking, are one order of magnitude smaller than JLAB measured values and the AKS14 prediction as well. We should mention here that the agreement in the order of magnitude between the experimental data and the AKS14 model arises from a combination of ingredients in which the experimental data and the AKS14 model differ significantly.

VII. CONCLUSIONS

The following conclusions can be drawn from the present study. In this article, we have conducted an investigation into the impact of symmetry breaking in polarized light sea quarks on the extraction of polarized PDFs. We analyze their effects on the polarized structure functions and their moments for both nucleons and nuclei, providing a detailed discussion. Additionally, we explore and present the implications of symmetry breaking on the sum rules and the components of the Lorentz color force. Furthermore, it is important to note that in our analysis, the polarized structure functions of nuclei are computed while considering the effective nuclear

		$\langle Q^2 \rangle$ [GeV ²]	JLAB16 [10]	NAAMY21 [25]	AKS14 [44]
d_2^n	$\times 10^{-5}$	3.21	$-421.0 \pm 79.0 \pm 82.0 \pm 8.0$	-125.566 ± 0.1712	-89.488 ± 2.333
	$\times 10^{-5}$	4.32	$-35.0 \pm 83.0 \pm 69.0 \pm 7.0$	-124.783 ± 4.809	-86.225 ± 1.806
f_2^n	$\times 10^{-3}$	3.21	$53.41 \pm 0.79 \pm 25.55$	9.972 ± 2.166	148.330 ± 25.851
	$\times 10^{-3}$	4.32	$49.66 \pm 0.83 \pm 25.99$	30.732 ± 28.246	219.473 ± 35.044
a_2^n	$\times 10^{-4}$	3.21	$8.552 \pm 1.761 \pm 6.125$	1.174 ± 0.01	3.953 ± 1.811
	$\times 10^{-4}$	4.32	$5.044 \pm 2.270 \pm 6.042$	1.632 ± 0.0003	3.754 ± 1.712

Table II: The values of d_2^n , a_2^n and f_2^n from JLAB [10] experimental data with statistical and systematic uncertainties. The values calculated by AKS14 and NAAMY21 polarized PDFs are also shown as well.

	$\langle Q^2 \rangle$ [GeV ²]	$F_E^{y,n}$ [MeV/fm]	$F_B^{y,n}$ [MeV/fm]
JLAB16 [10]	3.21	$-33.53 \pm 1.32 \pm 19.07$	$52.35 \pm 2.43 \pm 19.18$
JLAB16 [10]	4.32	$-36.48 \pm 1.38 \pm 19.38$	$38.04 \pm 2.55 \pm 19.46$
NAAMY21	3.21	-3.992 ± 3.264	2.207 ± 6.049
NAAMY21	4.32	-4.154 ± 6.332	5.256 ± 6.290
AKS14	3.21	-21.560 ± 3.796	22.350 ± 3.817
AKS14	4.32	-32.037 ± 5.150	32.798 ± 5.166

Table III: Measured magnetic and electric Lorentz color force components from JLAB [10] experiment along with statistical and systematic uncertainty. The calculated quantities using AKS14 and NAAMY21 polarized PDFs with statistical uncertainty are also shown for comparison.

modifications. This ensures a more accurate description of the nuclear effects on the polarized structure functions.

To investigate the impact of symmetry breaking in polarized light sea quarks, we compare the polarized PDFs of the AKS14, NAAMY21, DSSV09, and BB10 models with experimental data obtained from HERMES and COMPASS experiments. This comparison allows us to assess the agreement between the theoretical models considering symmetry breaking and the experimental data. The primary outcome of this comparison indicates slightly better agreement between the AKS14 model, which incorporates symmetry breaking, and the experimental data. This agreement is particularly notable for distributions involving strange and sea quarks. It suggests that considering symmetry breaking in the modeling of polarized light sea quarks leads to improved agreement with experimental observations.

In addition, we conduct a comparison of the polarized structure functions of the proton, neutron, and deuteron using calculations from the AKS14, NAAMY21, DSSV09, and BB10 models. This comparison is made with experimental data obtained from the E143 collaboration. The results obtained from the comparisons between data and theory indicate that when symmetry breaking is considered, the extracted predictions exhibit improved agreement with the experimental data, taking into account the associated uncertainties.

To investigate the impact of symmetry breaking on the nuclei structure function, we calculate the theoretical predictions of the polarized structure function $g_1^{3\text{He}}$ using the NAAMY21, AKS14, and KTA17 models at both NLO and NNLO accuracy in perturbative QCD.

These theoretical predictions are subsequently compared with experimental data from the E142 and JLAB

experiments. The findings of this comparison indicate that the polarized nuclei structure function calculated using the AKS14 polarized PDFs, which consider the symmetry breaking of light sea quarks, exhibits better agreement with the experimental data compared to other models. This agreement is particularly notable in the $0.1 \leq x \leq 0.4$ regions.

The same findings also apply to the cases of $g_2^{3\text{He}}$ and $x^2 g_1^{3\text{He}}$ structure functions. While the extracted polarized structure functions of nuclei from the AKS14 model demonstrate agreement with the experimental data, we should clarify that there are currently no available experimental data for $g_1^{3\text{H}}$. Furthermore, considering the uncertainties associated with the measurements of $g_2^{3\text{He}}$ and $x^2 g_1^{3\text{He}}$, it does not allow one to strongly prefer the AKS14 model over other models based solely on these measurements.

Our calculations demonstrate that the ratio η of the Bjorken sum rule and the extracted Lorentz color force components $F_B^{y,n}$ and $F_E^{y,n}$ from the AKS14 model are all in good agreement with the measured values as well.

In conclusion, the presented results provide evidence that a comprehensive understanding of the spin structure of nucleons, nuclei, sum rules, and Lorentz color force components of polarized structure functions can often be achieved when considering the breaking of both flavors SU(2) and SU(3) symmetry in a QCD analysis. By incorporating these symmetry-breaking effects, a more accurate description of the observed data and a better agreement between theory and experiment can be achieved.

ACKNOWLEDGMENTS

The authors acknowledge the financial support from the Iran National Science Foundation (INSF) under grant number 4013570. S. A. T. and H. K. are also thankful to the School of Particles and Accelerators, Institute for

Research in Fundamental Sciences (IPM). F. A. acknowledges the Farhangian University for providing support to conduct this research. The authors are grateful to Abolfazl Mirjalili for several useful comments. They would also like to express their gratitude to the anonymous referee for their valuable comments and suggestions, which have greatly contributed to enhancing the quality of this paper.

-
- [1] S. Amoroso, A. Apyan, N. Armesto, R. D. Ball, V. Bertone, C. Bissolotti, J. Bluemlein, R. Boughezal, G. Bozzi and D. Britzger, *et al.* [[arXiv:2203.13923 \[hep-ph\]](#)].
 - [2] T. J. Hobbs, P. M. Nadolsky, F. I. Olness and B. T. Wang, [[arXiv:2001.07862 \[hep-ph\]](#)].
 - [3] P. Agostini *et al.* [LHeC and FCC-he Study Group], *J. Phys. G* **48**, no.11, 110501 (2021). *J. Phys. G* **48**, no.11, 110501 (2021).
 - [4] A. Abada *et al.* [FCC], *Eur. Phys. J. C* **79**, no.6, 474 (2019).
 - [5] P. L. Anthony *et al.* [E142], *Phys. Rev. D* **54**, 6620-6650 (1996).
 - [6] K. Abe *et al.* [E143], *Phys. Rev. D* **58**, 112003 (1998).
 - [7] C. Adolph *et al.* [COMPASS], *Phys. Lett. B* **753**, 18-28 (2016).
 - [8] A. Airapetian *et al.* [HERMES], *Phys. Rev. D* **71**, 012003 (2005).
 - [9] X. Zheng *et al.* [Jefferson Lab Hall A], *Phys. Rev. Lett.* **92**, 012004 (2004).
 - [10] D. Flay *et al.* [Jefferson Lab Hall A], *Phys. Rev. D* **94**, no.5, 052003 (2016).
 - [11] J. J. Ethier and E. R. Nocera, *Ann. Rev. Nucl. Part. Sci.* **70**, 43-76 (2020).
 - [12] A. Deur, S. J. Brodsky and G. F. De Téramond, [[arXiv:1807.05250 \[hep-ph\]](#)].
 - [13] Y. Zhou *et al.* [Jefferson Lab Angular Momentum (JAM)], *Phys. Rev. D* **105**, no.7, 074022 (2022).
 - [14] H. W. Lin, E. R. Nocera, F. Olness, K. Orginos, J. Rojo, A. Accardi, C. Alexandrou, A. Bacchetta, G. Bozzi and J. W. Chen, *et al.* *Prog. Part. Nucl. Phys.* **100**, 107-160 (2018).
 - [15] D. F. Geesaman and P. E. Reimer, *Rept. Prog. Phys.* **82**, no.4, 046301 (2019).
 - [16] C. Ciofi degli Atti, S. Scopetta, E. Pace and G. Salme, *Phys. Rev. C* **48**, R968-R972 (1993).
 - [17] F. R. P. Bissey, A. W. Thomas and I. R. Afnan, *Phys. Rev. C* **64**, 024004 (2001).
 - [18] I. R. Afnan, F. R. P. Bissey, J. Gomez, A. T. Katramatou, S. Liuti, W. Melnitchouk, G. G. Petratos and A. W. Thomas, *Phys. Rev. C* **68**, 035201 (2003).
 - [19] S. Atashbar Tehrani and A. N. Khorramian, *JHEP* **07**, 048 (2007).
 - [20] A. N. Khorramian, S. Atashbar Tehrani, S. Taheri Monfared, F. Arbabifar and F. I. Olness, *Phys. Rev. D* **83**, 054017 (2011).
 - [21] F. Taghavi-Shahri, H. Khanpour, S. Atashbar Tehrani and Z. Alizadeh Yazdi, *Phys. Rev. D* **93**, no.11, 114024 (2016).
 - [22] S. Atashbar Tehrani, F. Taghavi-Shahri, A. Mirjalili and M. M. Yazdanpanah, *Phys. Rev. D* **87**, no.11, 114012 (2013). [erratum: *Phys. Rev. D* **88**, no.3, 039902 (2013)]
 - [23] H. Khanpour, S. T. Monfared and S. Atashbar Tehrani, *Phys. Rev. D* **95**, no.7, 074006 (2017).
 - [24] M. Salajegheh, S. M. Moosavi Nejad, M. Nejad, H. Khanpour and S. Atashbar Tehrani, *Phys. Rev. C* **97**, no.5, 055201 (2018).
 - [25] H. Nematollahi, P. Abolhadi, S. Atashbar, A. Mirjalili and M. M. Yazdanpanah, *Eur. Phys. J. C* **81**, no.1, 18 (2021).
 - [26] A. Mirjalili and S. Tehrani Atashbar, *Phys. Rev. D* **105**, no.7, 074023 (2022).
 - [27] A. V. Sidorov and D. B. Stamenov, *Mod. Phys. Lett. A* **21**, 1991-1998 (2006).
 - [28] E. Leader, A. V. Sidorov and D. B. Stamenov, *Phys. Rev. D* **91**, no.5, 054017 (2015).
 - [29] D. de Florian, G. A. Navarro and R. Sassot, *Phys. Rev. D* **71**, 094018 (2005).
 - [30] M. Gluck, E. Reya, M. Stratmann and W. Vogelsang, *Phys. Rev. D* **63**, 094005 (2001).
 - [31] J. Bluemlein and H. Bottcher, *Nucl. Phys. B* **636**, 225-263 (2002).
 - [32] D. de Florian, R. Sassot, M. Stratmann and W. Vogelsang, *Phys. Rev. Lett.* **101**, 072001 (2008).
 - [33] M. Hirai *et al.* [Asymmetry Analysis], *Nucl. Phys. B* **813**, 106-122 (2009).
 - [34] J. Bluemlein and H. Bottcher, *Nucl. Phys. B* **841**, 205-230 (2010).
 - [35] E. Leader, A. V. Sidorov and D. B. Stamenov, *Phys. Rev. D* **84**, 014002 (2011).
 - [36] E. Leader, A. V. Sidorov and D. B. Stamenov, [[arXiv:1007.4781 \[hep-ph\]](#)].
 - [37] E. Leader, A. V. Sidorov and D. B. Stamenov, *Phys. Rev. D* **80**, 054026 (2009).
 - [38] E. R. Nocera, *Phys. Lett. B* **742**, 117-125 (2015).
 - [39] H. Khanpour, S. T. Monfared and S. Atashbar Tehrani, *Phys. Rev. D* **96**, no.7, 074037 (2017).
 - [40] E. Leader, A. V. Sidorov and D. B. Stamenov, *Phys. Rev. D* **82**, 1140187 (2010).
 - [41] D. de Florian, R. Sassot, M. Stratmann and W. Vogelsang, *Phys. Rev. D* **80**, 034030 (2009).
 - [42] D. de Florian, R. Sassot, M. Stratmann and W. Vogelsang, *Phys. Rev. Lett.* **113**, no.1, 012001 (2014).
 - [43] R. D. Ball *et al.* [NNPDF], *Nucl. Phys. B* **874**, 36-84 (2013).
 - [44] F. Arbabifar, A. N. Khorramian and M. Soleymaninia, *Phys. Rev. D* **89**, no.3, 034006 (2014).
 - [45] A. Khorramian, E. Leader, D. B. Stamenov and A. Shabanpour, *Phys. Rev. D* **103**, no.5, 054003 (2021).
 - [46] A. Vogt, *Comput. Phys. Commun.* **170**, 65-92 (2005).
 - [47] B. Lampe and E. Reya, *Phys. Rept.* **332**, 1-163 (2000).

- [48] M. Lacombe, B. Loiseau, R. Vinh Mau, J. Cote, P. Pires and R. de Turreil, *Phys. Lett. B* **101**, 139 (1981).
- [49] W. W. Buck and F. Gross, *Phys. Rev. D* **20**, 2361 (1979).
- [50] M. J. Zuilhof and J. A. Tjon, *Phys. Rev. C* **22**, 2369 (1980).
- [51] G. Parisi and N. Surlas, *Nucl. Phys. B* **151**, 421-428 (1979).
- [52] T. J. Hou, J. Gao, T. J. Hobbs, K. Xie, S. Dulat, M. Guzzi, J. Huston, P. Nadolsky, J. Pumplin and C. Schmidt, *et al. Phys. Rev. D* **103**, no.1, 014013 (2021).
- [53] A. L. Kataev, G. Parente and A. V. Sidorov, *Phys. Part. Nucl.* **34**, 20 (2003). [*Fiz. Elem. Chast. Atom. Yadra* **34**, 43 (2003)] [*Phys. Part. Nucl.* **38**, no. 6, 827 (2007)].
- [54] A. L. Kataev, *JETP Lett.* **81**, 608 (2005). [*Pisma Zh. Eksp. Teor. Fiz.* **81**, 744 (2005)].
- [55] M. G. Alekseev *et al.* [COMPASS], *Phys. Lett. B* **693**, 227-235 (2010).
- [56] M. M. Yazdanpanah, A. Mirjalili, S. Atashbar Tehrani and F. Taghavi-Shahri, *Nucl. Phys. A* **831**, 243-262 (2009).
- [57] M. Lacombe, B. Loiseau, J. M. Richard, R. Vinh Mau, J. Cote, P. Pires and R. De Turreil, *Phys. Rev. C* **21**, 861-873 (1980).
- [58] L. Frankfurt, V. Guzey and M. Strikman, *Phys. Lett. B* **381**, 379-384 (1996).
- [59] T. Y. Saito, Y. Wu, S. Ishikawa and T. Sasakawa, *Phys. Lett. B* **242**, 12-16 (1990).
- [60] J. Carlson, D. O. Riska, R. Schiavilla and R. B. Wiringa, *Phys. Rev. C* **44**, 619-625 (1991).
- [61] C. Boros, V. A. Guzey, M. Strikman and A. W. Thomas, *Phys. Rev. D* **64**, 014025 (2001).
- [62] F. R. P. Bissey, V. A. Guzey, M. Strikman and A. W. Thomas, *Phys. Rev. C* **65**, 064317 (2002).
- [63] J. J. Ethier and W. Melnitchouk, *Phys. Rev. C* **88**, no.5, 054001 (2013).
- [64] X. Zheng *et al.* [Jefferson Lab Hall A], *Phys. Rev. C* **70**, 065207 (2004).
- [65] K. Kramer, Ph.D. thesis, College of William and Mary, 2003.
- [66] S. Wandzura and F. Wilczek, *Phys. Lett. B* **72**, 195-198 (1977).
- [67] B. Budick, J. S. Chen and H. Lin, *Phys. Rev. Lett.* **67**, 2630-2633 (1991).
- [68] J. D. Bjorken, *Phys. Rev.* **148**, 1467-1478 (1966).
- [69] C. Patrignani *et al.* [Particle Data Group], *Chin. Phys. C* **40**, no.10, 100001 (2016).
- [70] J. Blumlein and N. Kochelev, *Nucl. Phys. B* **498**, 285-309 (1997).
- [71] P. L. Anthony *et al.* [E155], *Phys. Lett. B* **553**, 18-24 (2003).
- [72] M. Burkardt, *Phys. Rev. D* **88**, 114502 (2013).
- [73] A. L. Kataev, *Phys. Rev. D* **50**, R5469-R5472 (1994).
- [74] S. A. Larin, T. van Ritbergen and J. A. M. Vermaseren, *Phys. Lett. B* **404**, 153-160 (1997).
- [75] M. Osipenko, W. Melnitchouk, S. Simula, P. E. Bosted, V. Burkert, M. E. Christy, K. Griffioen, C. Keppel and S. E. Kuhn, *Phys. Lett. B* **609**, 259-264 (2005).
- [76] Z. E. Meziani, W. Melnitchouk, J. P. Chen, S. Choi, T. Averett, G. Cates, C. W. de Jager, A. Deur, H. Gao and F. Garibaldi, *et al. Phys. Lett. B* **613**, 148-153 (2005).